magnetochemistry

MDPI

Article

An Effect of Fe^{3+} Ion Substitution for Cr^{3+} in the Octahedral Sites of $FeCr_2O_4$ Multiferroic Spinel: Mössbauer Spectroscopy Study

Almaz L. Zinnatullin *, Mikhail A. Cherosov, Ruslan G. Batulin, Farit G. Vagizov and Roman V. Yusupov

Institute of Physics, Kazan Federal University, Kazan 420008, Russia
* Correspondence: allzinnatullin@kpfu.ru

Abstract: We present the results of a successful synthesis and investigation of polycrystalline $Fe^{2+}(Cr^{3+}, Fe^{3+})_2O_4$ powder, where 1/8 part of the Cr^{3+} ions in the octahedral sites is substituted by the Fe^{3+} ones. It is shown that under such doping, the material retains the cubic spinel structure characteristic of the parent $FeCr_2O_4$ compound. However, the values of the critical temperatures have changed. Both the orbital and magnetic orderings occur at about 120 K, and magnetic structure rearrangement associated with an onset of spiral modulation takes place at 26 K. Mössbauer studies in a wide temperature range make it possible to accurately control the content of iron ions, their valence and magnetic states, and local environment, therefore, allowing a deeper understanding of the features of the revealed transformations.

Keywords: iron chromite; Mössbauer spectroscopy; multiferroics; spinel

Citation: Zinnatullin, A.L.; Cherosov, M.A.; Batulin, R.G.; Vagizov, F.G.; Yusupov, R.V. An Effect of Fe^{3+} Ion Substitution for Cr^{3+} in the Octahedral Sites of $FeCr_2O_4$ Multiferroic Spinel: Mössbauer Spectroscopy Study. *Magnetochemistry* **2023**, *9*, 98. https://doi.org/10.3390/magnetochemistry9040098

Academic Editor: Shengcan Ma

Received: 7 March 2023
Revised: 27 March 2023
Accepted: 29 March 2023
Published: 2 April 2023

1. Introduction

The spinel-structure $FeCr_2O_4$ compound attracts the attention of researchers due to a unique combination of properties [1,2]. This compound reveals a sequence of phase transitions with temperature lowering, including the orbital ordering at 138 K, the magnetic ordering at 65 K to the collinear ferrimagnetic state, and the establishment of spin-modulated structure at 38.5 K [3]. Moreover, this iron chromite possesses the magnetoelectric coupling, i.e., displays multiferroic properties [4]. Since the ferroelectric properties arise with the magnetic ordering, this compound is the representative of the type-II multiferroics [5]. The general interest in multiferroic materials lies in their ability to control the magnetization of a compound using an applied electric field and *vice versa*, i.e., electric polarization by an external magnetic field. Hence, these materials are promising for the development of new multifunctional devices such as, for instance, magnetic field sensors, non-volatile random-access memory, and multi-state memory elements [6,7].

The substitution of Cr^{3+} ions in $FeCr_2O_4$ by Fe^{3+} ones significantly modifies the properties of a material. It was shown that, upon an increase in the x value in $Fe^{2+}Cr^{3+}{}_{2-x}Fe^{3+}{}_xO_4$, three regions in the room-temperature phase diagram exist [8–10]. In the first region ($x < 0.68$), the crystal retains the normal spinel structure. The room-temperature lattice cell parameter value increases with an increase in the ferric ion content. At the same time, the magnetic moment decreases. In the second region ($0.75 < x < 1.38$), the reverse behaviors are observed, i.e., with an increase in x, the unit cell parameter decreases while the magnetic moment rises. Moreover, in this region, a partial inversion in the site distribution of the ferric Fe^{3+} and ferrous Fe^{2+} ions starts to manifest itself. Both the lattice cell parameter and the magnetic moment grow in the third region ($1.50 < x < 2.0$), approaching the magnetite Fe_3O_4 at the end. The magnetite has the inverse spinel structure, in which the tetrahedral sites are occupied by the ferric ions, and the octahedral ones by the ferric and ferrous ions in equal fractions. It should be noted that the magnetic ordering temperature also rises

upon the substitution of Cr^{3+} by Fe^{3+} ions and becomes higher than room temperature at $x \approx 0.9$ [9].

The low-temperature magnetic phase diagram is more complex. A recent study shows that the first region, as mentioned above, is split into two with $x < 0.3$ and $0.3 < x < 0.7$ [11]. For $x < 0.3$, the compound undergoes a sequence of transitions with decreasing temperature, namely, from the paramagnetic cubic phase to the paramagnetic tetragonal (with $a/c > 1$) to the ferrimagnetic orthorhombic phase, as well as the onset of conical spin order. For $0.3 < x < 0.7$, the transitions have the same pattern with a difference in the tetragonal phase, which is ferrimagnetic and $a/c < 1$. The corresponding critical temperatures are defined by the x value. Near a boundary between these two regions in the low-temperature magnetic phase diagram, i.e., at $x \approx 0.3$, the critical temperatures of the phase transitions nearly coincide. According to Ref. [12], for the composition of $x \approx 0.25$, an almost direct transition from the paramagnetic cubic phase to the ferrimagnetic orthorhombic phase is observed.

Another phenomenon, which is manifested in the $Fe^{2+}(Cr^{3+}{}_{1-x}\ Fe^{3+}{}_{x})_2O_4$ row, is charge hopping [9]. It develops under an inversion of the Fe^{2+}-Fe^{3+} site distribution, i.e., in the second region. However, since the ferric and the ferrous ions both have a tendency to occupy the tetrahedral and the octahedral sites in the spinel structure, traces of charge hopping may be found in the first region as well.

In this work, we study the effect of the ferric ion substitution in $FeCr_2O_4$ spinel. We have chosen the composition of $Fe^{2+}Cr^{3+}{}_{1.75}Fe^{3+}{}_{0.25}O_4$ for the following reasons. First, the ferric ions ($S = 5/2$) have a larger magnetic moment compared with the Cr^{3+} ones ($S = 3/2$). Consequently, such doping of the octahedral sites should increase the magnetization of the sublattice. However, to directly compare the compound's properties with those of the stoichiometric $FeCr_2O_4$, it is necessary to preserve the normal spinel structure, i.e., x should be less than 0.68. Moreover, we tried to avoid charge hopping, and, therefore, used an even lower content of ferric ions. Finally, as noted above, for this composition, a direct transition from the cubic paramagnetic to the orthorhombic ferrimagnetic phase is expected, preventing the transition to the paramagnetic or ferrimagnetic states with tetragonal lattice symmetry. Another advantage of the substitution of octahedral sites with iron ions is the possibility of studying the hyperfine interactions within this sublattice with Mössbauer spectroscopy. The given substitution of Cr^{3+} sites by Fe^{3+} ions requires precise control of the amount of Fe^{2+} and Fe^{3+} ions in the synthesized compound. For this purpose, an original synthesis route based on the use of iron (II) oxalate dihydrate as a starting reagent is proposed.

2. Experimental Part

The polycrystalline $Fe^{2+}Cr^{3+}{}_{1.75}Fe^{3+}{}_{0.25}O_4$ sample was synthesized via the solid-state route. To achieve the desired composition of the product, the molar fractions of the initial components were adjusted to fit the reaction:

$$8{\cdot}Fe^{2+}O + Fe^{3+}{}_2O_3 + 7{\cdot}Cr_2O_3 \rightarrow 8{\cdot}Fe^{2+}Cr_{1.75}Fe^{3+}{}_{0.25}O_4.$$

Fe_2O_3 (Alfa Aesar, 99%) and Cr_2O_3 (Alfa Aesar, 99%) powders as well as the $FeC_2O_4{\cdot}2H_2O$ (LLC "Component-Reaktiv", 99%) (iron (II) oxalate dihydrate) powder as the source of FeO were used as starting reagents. The required weight of iron (II) oxalate dihydrate was adjusted accounting for the thermal gravimetric analysis (TGA) data. According to TGA measurements [13,14], upon heating, iron (II) oxalate dihydrate first releases water molecules (at ~175 °C) and then, in the range of 200–300 °C, decomposes following the simplified reaction of

$$FeC_2O_4 \rightarrow FeO + CO_2 + CO.$$

Carbon monoxide released during decomposition inhibits the oxidation of FeO and, thus, preserves the iron ions in the ferrous state. However, it should be noted that the decomposition reactions for iron (II) oxalate dihydrate in the presence of its conversion gases are more complicated [15].

The starting powders were mixed in the stoichiometric ratio and then thoroughly ground and mixed in the air for 3 h in an agate mortar. The mixture in the alumina crucible was placed in the vertical tube furnace chamber. The chamber was pre-evacuated to 10^{-2} mbar of pressure several times with the spiral vacuum pump and filled with pure Ar (99.9998%). The synthesis took place at the temperature of 1400 °C for 12 h under a weak argon flow (less than 0.01 L/min) with slight excess pressure (less than 0.01 bar) in the chamber.

The phase composition of a synthesized compound and the crystal structure of the product were studied with powder X-ray diffraction (XRD). The XRD measurements were carried out at room temperature (RT) with the Bruker D8 Advance diffractometer equipped with the Cu-Kα radiation tube. For the measurements, samples were carefully ground in an agate mortar to a fine powder state.

Mössbauer effect studies were carried out in the transmission geometry with the conventional WissEl spectrometer operating in the constant acceleration mode. The spectra were measured within the temperature range of 5–295 K in CFICEV helium flow cryostat (ICEOxford) with a temperature accuracy of $\pm$0.1 K monitored by a CryoCon 32B controller. ^{57}Co(Rh) source (purchased from RITVERC JSC, St. Petersburg, Russia) with an activity of about 40 mCi. The spectrometer velocity scale was calibrated using the spectrum of thin iron foil. The spectra were fitted using the SpectrRelax 2.1 software [16]. Values of the center shift are reported versus the center shift of α-Fe spectrum at RT.

The magnetization of the synthesized compound as a function of the magnetic field and temperature was measured using the Physical Property Measurement System (PPMS-9) (Quantum Design) utilizing the vibrating sample magnetometry (VSM) option. Magnetic studies were carried out in the temperature range of 5–400 K applying the magnetic fields up to 9 T.

The measurements of specific heat at a constant pressure (C_p) in a zero applied magnetic field in the temperature range of 10–200 K were carried out with a heat capacity option on the PPMS-9 using a 2τ relaxation method.

3. Results and Discussion

3.1. Powder X-ray Diffraction

The powder XRD pattern of the polycrystalline $Fe^{2+}Cr^{3+}{}_{1.75}Fe^{3+}{}_{0.25}O_4$ sample at room temperature (RT) and its Rietveld refined model curve are shown in Figure 1.

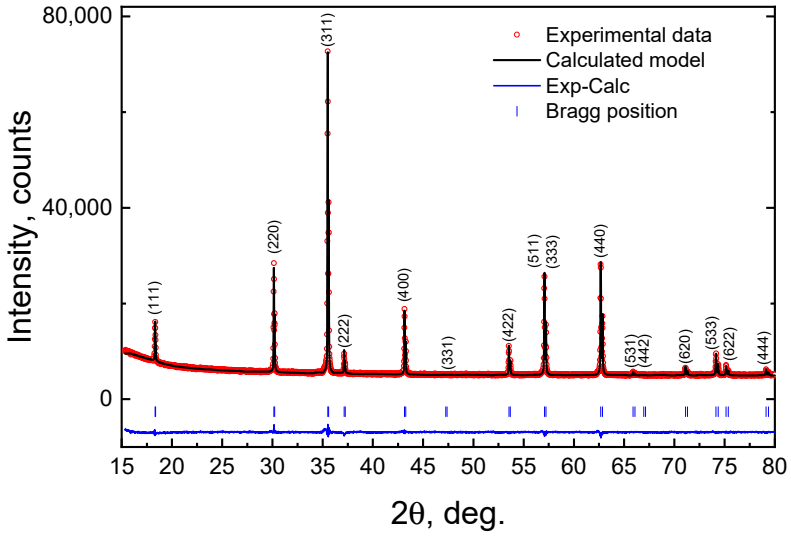

Figure 1. The powder XRD pattern of the polycrystalline $Fe^{2+}Cr^{3+}{}_{1.75}Fe^{3+}{}_{0.25}O_4$ sample at room temperature (red circles) and its Rietveld refined model curve (black curve).

The data were analyzed via standard Rietveld refinement using the FULLPROF software [17]. Reflexes attributed to the spinel structure were observed. We could not detect any impurity phase in the studied sample. The structural analysis confirmed a formation of the cubic structure belonging to the $Fd\bar{3}m$ space group with the lattice parameter of a = 8.379(1) Å. This value matches well with the one reported earlier [9].

3.2. Magnetic Properties

The temperature dependencies of the sample magnetization recorded in the zero-field-cooled (ZFC) and field-cooled (FC) modes are shown in Figure 2a. Both curves were recorded upon warming in the magnetic field of 100 Oe. The sample reveals a paramagnetic behavior down to 126 K. The magnetization follows the Curie–Weiss law down to 200 K, and the estimated Curie–Weiss parameter (temperature) is $\theta_{CW} = -320$ K (see the inset in Figure 2a). The negative value of θ_{CW} indicates an essentially antiferromagnetic character of the exchange interactions between the magnetic ions.

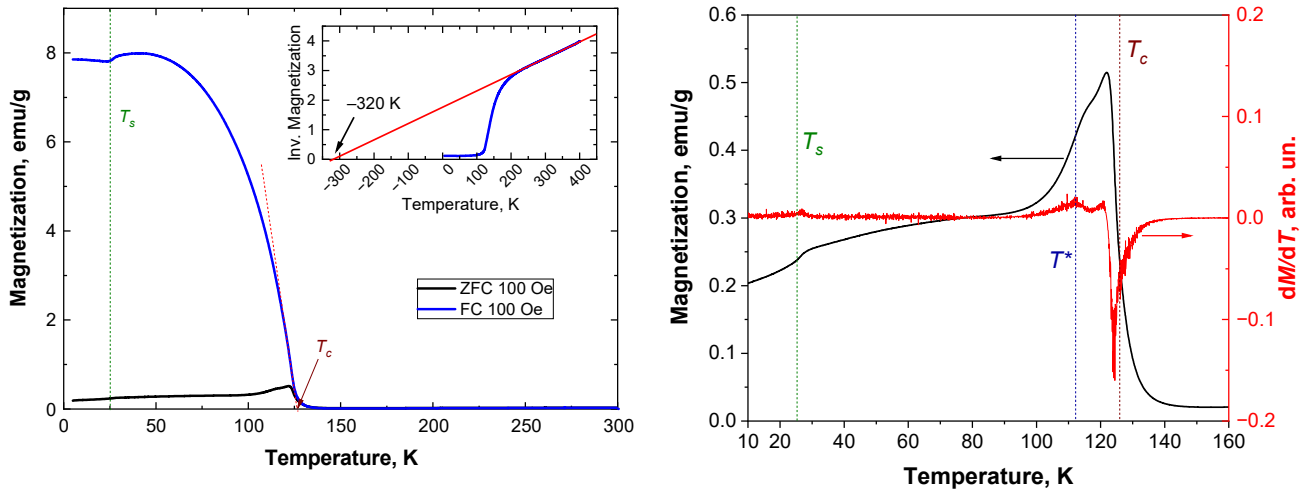

Figure 2. (**a**) Temperature dependencies of the magnetization recorded in the zero-field-cooled (ZFC—black curve) and in the field-cooled (FC—blue curve) regimes. (**b**) ZFC magnetization (black curve) and its first derivative (red curve). The inset in (**a**) panel shows the temperature dependence of inverse magnetization.

With a further decrease in temperature, the magnetization deviates from this law, most probably due to the development of magnetic correlations. At T_c = 126 K, the sample undergoes the magnetic phase transition. This transition is associated with an establishment of the long-range magnetic order in the studied sample [11]. The so-called frustration factor, defined as $f = |\theta_{CW}|/T_c$, equals ~2.5. This value is smaller than that of a parent $FeCr_2O_4$ compound, for which the reported value is f = 5 [18]. The frustration arises from the octahedral sublattice, which has a pyrochlore-type geometrical arrangement. Partial substitution of the Cr^{3+} ions by the Fe^{3+} breaks this geometrical balance, and the magnetic ordering temperature rises, decreasing the frustration factor.

The significant difference between ZFC and FC curves reflects an occurrence of magnetic irreversibility in the studied sample below the T_c. It should be noted, however, that the observed transition is complex. In Figure 2b, the first derivative of the ZFC curve is depicted. It is seen that the magnetic phase transition is accompanied by another transformation at ~112 K, marked as T^*. This temperature is specified in the maximum dM/dT curve. However, this feature is subtle in the FC curve. The origin of this transformation is unclear. On the one hand, it may be related to the domain wall pinning effect. For instance, the broad maximum in the ZFC curve observed in $MnCo_2O_4$ was associated with the domain pinning effect in one study [19]. On the other hand, as shown below based on

the analysis of Mössbauer hyperfine fields, the long-range magnetic ordering is established within two sublattices at slightly different temperatures, namely, in the tetrahedral (*A*) sublattice at 121 K and in the octahedral (*B*) sublattice at 111 K. These temperatures match well with the anomalies in the ZFC curve. Therefore, one may suppose that they are related to the magnetization of the two sublattices in the sample.

With further cooling, another magnetic transition emerges at T_s = 26 K. Below this temperature, a decrease in the sample magnetization was observed. This decrease is commonly associated with an onset of a spiral-like modulation of the magnetic moments [1].

In Figure 3, the field dependencies of the magnetization recorded at 5, 50, and 300 K are presented. Below the magnetic phase transition temperature, these dependencies have a clear hysteretic behavior, while above the T_c the dependence is linear typical for the paramagnetic state. In the external magnetic field of 9 T, the magnetization reaches the values of 0.76 μ_B/f.u. and 0.72 μ_B/f.u. at 50 K and 5 K, respectively. These values are somewhat smaller than the value of 0.8 μ_B/f.u. that was reported for $FeCr_2O_4$ and ascribed to the Yafet–Kittel-type canted spin arrangement [20,21]. In this case, the *A* sublattice has the dominant magnetic moment, while the magnetic moments in the *B* sublattice are located at some angle to each other and the resulting magnetization of this sublattice is smaller. The replacement of part of the Cr^{3+} ions ($S = 3/2$) by the Fe^{3+} ones ($S = 5/2$) in the *B* sublattice enhances the magnetization of the latter. Since the *B*-sublattice magnetization is aligned antiparallel to that of the *A* sublattice, the total magnetization of the studied spinel should decrease upon such doping.

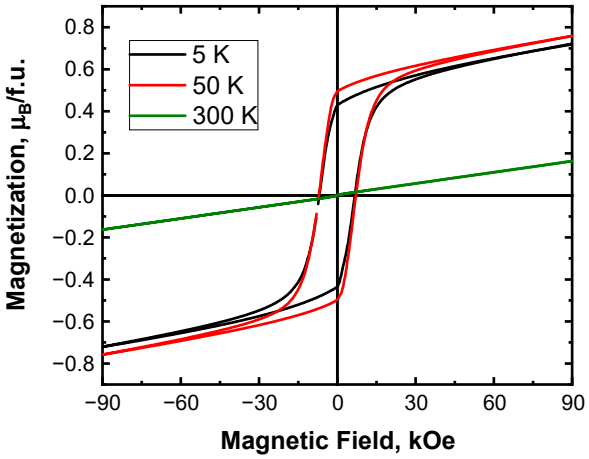

Figure 3. The magnetization versus applied magnetic field of the studied sample recorded at 5 K (black curve), 50 K (red curve), and 300 K (green curve).

The coercivity of the sample has the same value at 5 and 50 K and is about 7000 Oe. This value is notably higher than for a parent $FeCr_2O_4$, for which a coercivity of 3000 Oe at 4.2 and 20.4 K was reported [21]. We suppose that the higher value of the coercivity field is due to an increase in the magnetic anisotropy of Fe^{3+}-substituted $FeCr_2O_4$, compared with the unsubstituted one.

3.3. Specific Heat Studies

The temperature dependence of the specific heat at a constant pressure (C_p) is depicted in Figure 4. There are two anomalies in this curve that match the observed magnetic transformations in the sample. No other anomalies could be observed. The peak centered at 118 K is relatively broad. We suppose this is due to a coincidence of transformations occurring in the system, including the Jahn–Teller (orbital ordering) transition and the magnetic transition. The complex origin of the latter was noted above, and this may also lead to the additional broadening of this peak in the $C_p(T)$ curve.

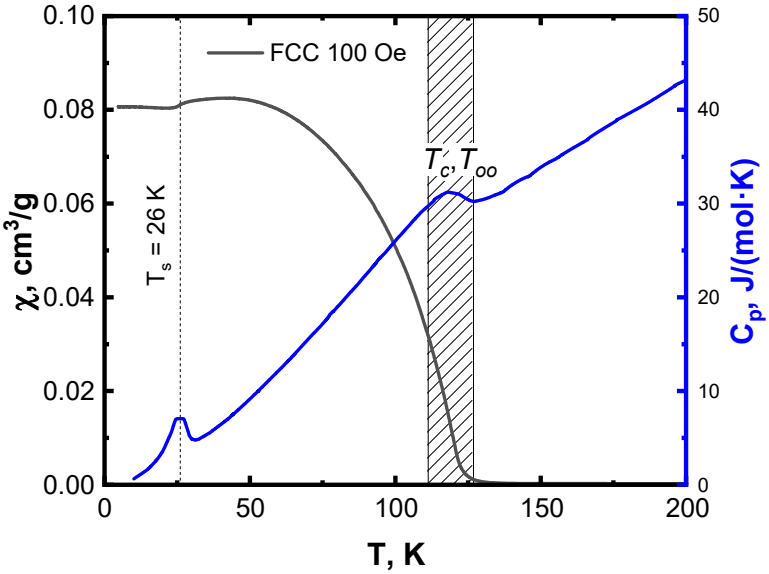

Figure 4. The temperature dependencies of the specific heat (blue curve) and the magnetic susceptibility recorded in the FCC regime (black curve) for $Fe^{2+}Cr^{3+}_{1.75}Fe^{3+}_{0.25}O_4$.

3.4. Mössbauer Effect Studies

In Figure 5, the representative Mössbauer spectra of the sample recorded at 295, 40, and 5 K are shown. The room-temperature (RT) spectrum was processed within a model of two doublets. The first doublet, which is shown in Figure 5a by the dark-green curve, has a center shift (*CS*) of 0.930(5) mm/s and a quadrupole splitting (*QS*) of 0.26(1) mm/s. The second one, presented by the light-green curve in the RT spectrum, is characterized by *CS* = 0.355(1) mm/s and *QS* = 0.47(1) mm/s. Based on these hyperfine parameters, we assign these two doublets to the high-spin ferrous and the high-spin ferric ions in the tetrahedral and the octahedral oxygen surroundings, respectively. The relative areas of the components are 78(1)% for the ferrous doublet and 22(1)% for the ferric one. The ratio of the spectra areas is ~4/1, indicating a target composition of the Fe^{3+}-substituted $FeCr_2O_4$ since the Lamb–Mössbauer factors are almost equal for *A* and *B* sites in the spinel structure [9]. No other iron-bearing phases were observed in the spectrum.

With a decrease in temperature, the center shift for both components increases due to the second-order Doppler effect. However, there is a difference in the temperature behavior of the *QS* values. For the ferrous component, the *QS* reveals a strong temperature dependence, while, for the ferric one, it is almost temperature-independent. Generally, the electric field gradient (EFG), which causes and determines the quadrupole splitting, is the sum of two parts, namely, the valence and the lattice contributions [22,23]. The former is defined by the lack of spherical symmetry in the occupation of iron electron orbitals, while the latter is determined by the charge distribution in the vicinity of an iron ion. The valence contribution is strongly temperature-dependent, while, for the lattice part of the EFG, a noticeable dependence of *QS*(*T*) is not characteristic. The high-spin Fe^{3+} ions have a $3d^5$ electron configuration. These five electrons are distributed over the five 3*d* orbitals, and their total contribution to the EFG is zero. Thus, the *QS* is defined in this case by the lattice part only. The sixth electron in the 3*d* shell in the high-spin Fe^{2+} ion ($3d^6$ electron configuration) breaks the spherical symmetry of the iron valence orbitals' occupation. In the cubic crystal field, 3*d* orbitals of ferrous iron in the surrounding tetrahedral oxygen split into the lower orbital doublet and upper triplet. In the presence of a dynamic Jahn–Teller effect, the ground state has a vibronic character, and the system fluctuates between the tetragonally distorted configurations. These fluctuations are thermally activated, and, therefore, the relaxation frequency is temperature-dependent. Consequently, the temperature dependence of the *QS* originates from the vibronic dynamics of the system.

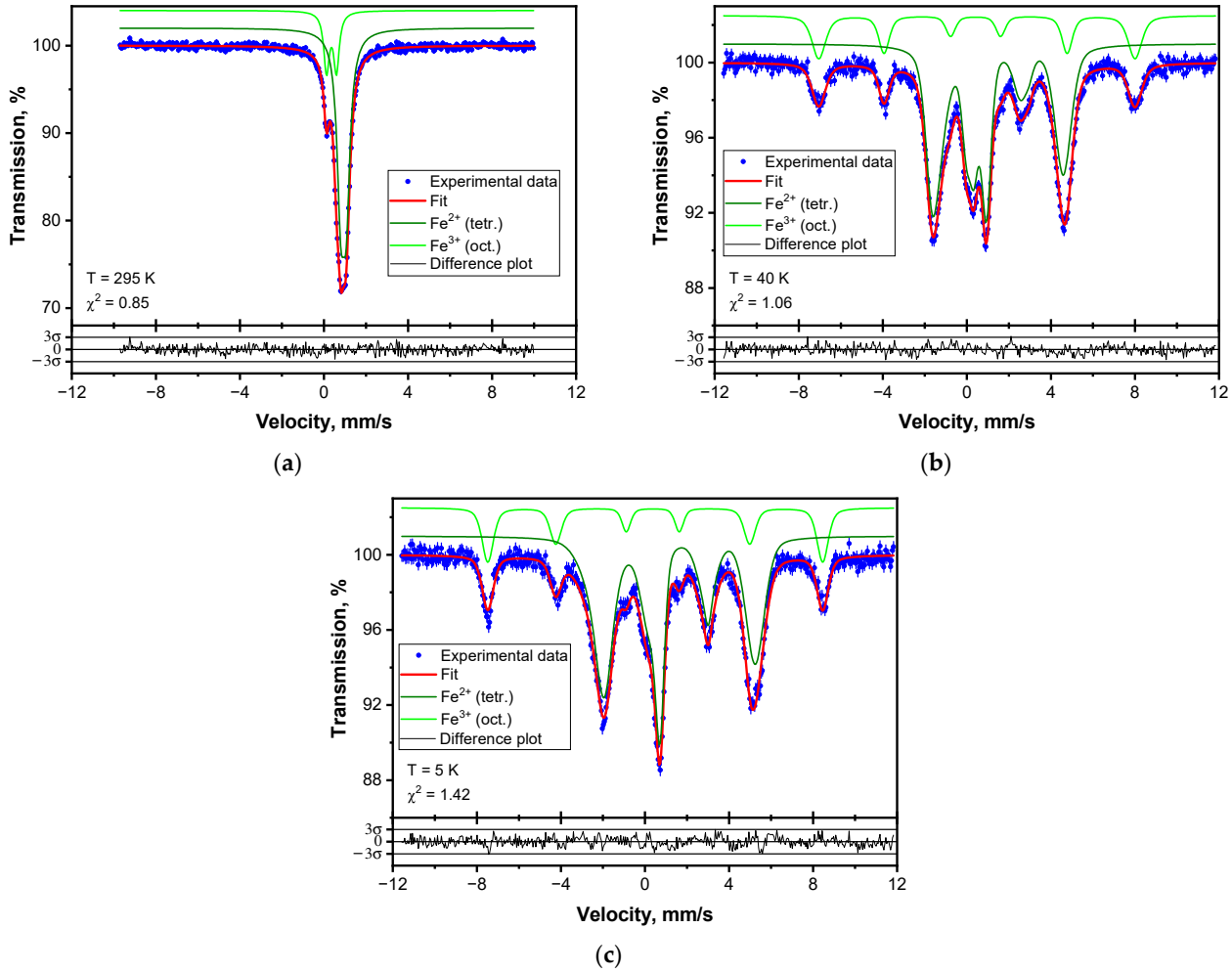

Figure 5. Mössbauer spectra of $Fe^{2+}Cr^{3+}_{1.75}Fe^{3+}_{0.25}O_4$ sample recorded at (**a**)—295 K, (**b**)—40 K, and (**c**)—5 K, and their fitting model curves. The residuals between experimental data and the fitting curves are shown at the bottom in the units of the statistical error.

Below 130 K, magnetic splitting of the components develops. The spectrum assigned to the ferric ions was processed by the Zeeman sextet. At the same time, in the case of the component assigned to the ferrous ones, it is necessary to consider the full Hamiltonian of combined hyperfine interactions, since the quadrupole and magnetic interactions are of the same order. In this case, angles between the hyperfine magnetic field direction and the principal axis of the EFG tensor as well as the asymmetry of the EFG have a crucial impact on the shape of the corresponding spectral component. We have found that, in the frame of the principal axes of the EFG tensor, the polar angle θ equals $\pi/2$ for all spectra (Figure 6a). At the same time, pronounced temperature dependencies were observed for the azimuthal angle φ and the EFG asymmetry parameter $\eta = (V_{xx} - V_{yy})/V_{zz}$, where V_{xx}, V_{yy}, and V_{zz} are the diagonal elements of the EFG tensor in its principal axes frame. With the temperature decrease from 120 K down to 40 K, the former increases from ~$\pi/4$ to ~$\pi/3$, while the latter is almost constant and equals ~ 0.55. However, at 5 K, η was found to be zero, and, consequently, the φ angle was not determined.

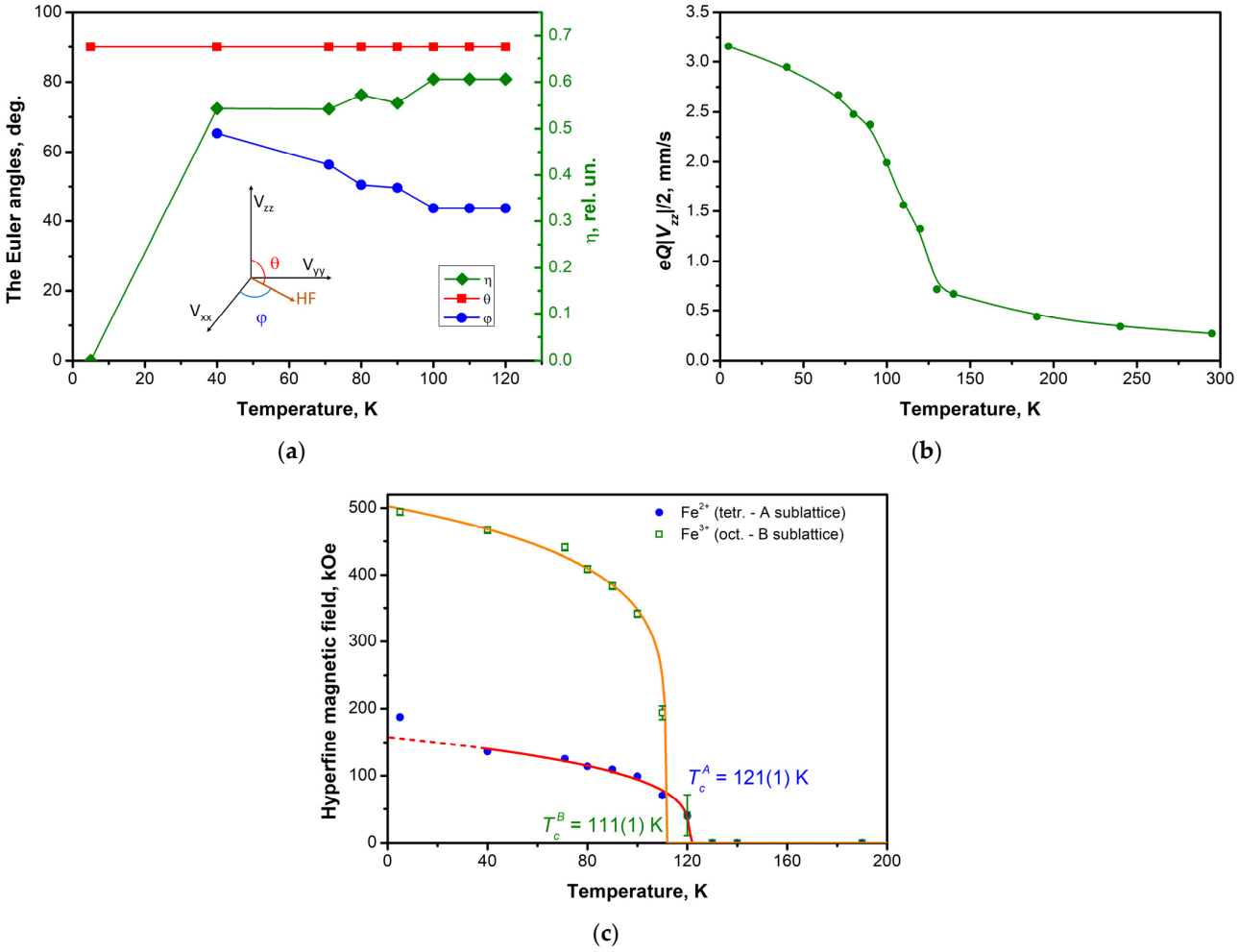

Figure 6. Temperature dependencies of Mössbauer spectra parameters: (**a**) the Euler angles θ (red curve) and φ (blue curve), the electric field gradient asymmetry parameter η (green curve) for ferrous ions; (**b**) the V_{zz} component of the electric field gradient for ferrous ions; (**c**) hyperfine magnetic fields on the ^{57}Fe nuclei for the ferrous (blue points—experimental data, red curve—the model fit using Equation (1)) and ferric (green points and orange curve, respectively) ion components. The inset in (**a**) shows a schematic direction of the hyperfine magnetic field (HF) in the EFG tensor principal axes frame.

The V_{zz} component of the EFG has a negative sign. Its absolute value markedly increases below 130 K (Figure 6b). This fact should be associated with the macroscopic structural distortion caused by the transition long-range orbitally ordered state. Such an ordering stabilizes the $|3z^2\rangle$ or $|x^2 - y^2\rangle$ type orbitals. The former has a negative contribution to the EFG, while the latter, has a positive one. Consequently, the negative sign of V_{zz} indicates that the ground state is of the $|3z^2\rangle$ type. Notable temperature dependence of the V_{zz} is related to the thermal population of the $|x^2 - y^2\rangle$-type states. Besides the orbital ordering, lattice distortions driven by the exchange interactions may also affect the splitting between these orbital levels and, consequently, the temperature dependence of the V_{zz}.

The temperature dependencies of the hyperfine magnetic fields at the ^{57}Fe nuclei (*HF*) for both components are shown in Figure 6c. These dependencies *HF*(*T*), except for the lowest temperature point for the ferrous component, were fitted using the following power law expression:

$$HF(T) = HF(0) \cdot \left(1 - \frac{T}{T_c}\right)^{\beta}, \quad (1)$$

where $HF(0)$ is the hyperfine magnetic field at 0 K, T_c—is the critical temperature, and β is the critical exponent. We have found that, for the ferrous ion component, $HF^A(0)$ = 158(6) kOe, β^A = 0.30(3), and $T_c{}^A$ = 121(1) K, while for the ferric one, $HF^B(0)$ = 503(13) kOe, β^B = 0.16(3), and $T_c{}^B$ = 111(1) K.

The long-range magnetic order sets in the *A* sublattice at 121 K. This temperature coincides with the observed critical temperature observed in the magnetization measurements. The value of the critical exponent β^A is characteristic of three-dimensional magnetic systems. For instance, β = 0.31–0.33 for the 3D-Ising systems [24]. The hyperfine magnetic field at 0 K found by the extrapolation of the power law dependence is even less than that observed experimentally at 5 K.. An increase in the *HF* below the temperature of the spiral spin modulation onset was also reported for the parent $FeCr_2O_4$ spinel [25].

In the case of the *B*-sublattice magnetization, we have found that the long-range magnetic order sets in at 111 K. This temperature is 10 K less than that of the *A* sublattice. Moreover, at this temperature, we observed an anomaly in the ZFC magnetization curve. Therefore, we conclude that two sublattices in our sample magnetically order at slightly different temperatures. However, the magnetic splitting of the ferric component was observed at 120 K. We suppose that this hyperfine field transferred from the *A* sublattice is not related to the establishment of the magnetic order in the *B* sublattice. The estimated value of $HF^B(0)$ is typical for the ferric ions in oxides. However, the critical exponent β^B is markedly lower than the value for the *A* sublattice. We relate this fact to the structural peculiarities of the *B* sublattice. It is well known that the *B* sublattice has a pyrochlore-type arrangement. This structure causes the geometric frustration. We suppose that the frustration may lead to such values of β. Indeed, β = 0.18(2) was observed in highly frustrated pyrochlore antiferromagnets [26].

4. Conclusions

We synthesized and investigated the $FeCr_2O_4$ compound, in which 1/8 part of the Cr^{3+} ions in the octahedral B sites are substituted by the Fe^{3+} ions. Such substitution preserves the normal spinel structure of the parent $FeCr_2O_4$ compound. We find that the Fe^{3+} ions occupy only the octahedral B sites, and no trace of charge hopping between the iron ions was detected. The Fe^{3+}-ion substitution markedly modifies the critical transition temperatures and reduces the frustration factor of the compound. Moreover, we demonstrate that the critical temperatures of the long-range magnetic ordering, as well as the critical behaviors of the magnetization within two sublattices, differ.

Author Contributions: Conceptualization, R.G.B., F.G.V. and R.V.Y.; methodology, R.G.B., F.G.V. and R.V.Y.; formal analysis, A.L.Z., M.A.C., F.G.V. and R.V.Y.; investigation, A.L.Z., M.A.C., R.G.B., F.G.V. and R.V.Y.; resources, R.G.B., F.G.V. and R.V.Y.; writing—original draft preparation, A.L.Z., M.A.C., F.G.V. and R.V.Y.; writing—review and editing, A.L.Z., M.A.C., R.G.B., F.G.V. and R.V.Y.; visualization, A.L.Z., M.A.C. and F.G.V.; supervision, F.G.V. and R.V.Y. All authors have read and agreed to the published version of the manuscript.

Funding: The synthesis, magnetometry, and heat capacity measurements were supported by the Russian Science Foundation, project No. 19-12-00244.

Institutional Review Board Statement: Not applicable.

Informed Consent Statement: Not applicable.

Data Availability Statement: The data presented in this study are available on request from the corresponding author. The data are not publicly available due to privacy restrictions.

Acknowledgments: The Mössbauer spectroscopy studies were funded by the Kazan Federal University Strategic Academic Leadership Program (PRIORITY-2030).

Conflicts of Interest: The authors declare no conflict of interest. The funders had no role in the design of the study; in the collection, analyses, or interpretation of data; in the writing of the manuscript; or in the decision to publish the results.

References

1. Tsurkan, V.; von Nidda, H.-A.K.; Deisenhofer, J.; Lunkenheimer, P.; Loidl, A. On the Complexity of Spinels: Magnetic, Electronic, and Polar Ground States. *Phys. Rep.* **2021**, *926*, 1–86. [CrossRef]
2. Yusupov, R.V.; Cherosov, M.A.; Gabbasov, B.F.; Vasin, K.V.; Batulin, R.G.; Kiyamov, A.G.; Eremin, M.V. Magnetic Irreversibilities and Nonreciprocity of the Microwave Absorption of $FeCr_2O_4$ Spinel. *JETP Lett.* **2022**, *115*, 167–173. [CrossRef]
3. Batulin, R.; Cherosov, M.; Kiiamov, A.; Zinnatullin, A.; Vagizov, F.; Tayurskii, D.; Yusupov, R. Synthesis and Single Crystal Growth by Floating Zone Technique of $FeCr_2O_4$ Multiferroic Spinel: Its Structure, Composition, and Magnetic Properties. *Magnetochemistry* **2022**, *8*, 86. [CrossRef]
4. Singh, K.; Maignan, A.; Simon, C.; Martin, C. $FeCr_2O_4$ and $CoCr_2O_4$ Spinels: Multiferroicity in the Collinear Magnetic State? *Appl. Phys. Lett.* **2011**, *99*, 172903. [CrossRef]
5. Khomskii, D. Classifying Multiferroics: Mechanisms and Effects. *Physics* **2009**, *2*, 20. [CrossRef]
6. Wang, J. (Ed.) *Multiferroic Materials: Properties, Techniques, and Applications*; CRC Press: Boca Raton, FL, USA, 2016. [CrossRef]
7. Cano, A.; Meier, D.; Trassin, M. (Eds.) *Multiferroics: Fundamentals and Applications*; De Gruyter: Berlin/Boston, MA, USA, 2021. [CrossRef]
8. Francombe, M.H. Lattice Changes in Spinel-Type Iron Chromites. *J. Phys. Chem. Solids* **1957**, *3*, 37–43. [CrossRef]
9. Robbins, M.; Wertheim, G.K.; Sherwood, R.C.; Buchanan, D.N.E. Magnetic Properties and Site Distributions in the System $FeCr_2O_4$-Fe_3O_4($Fe^{2+}Cr_{2-x}Fe_x{}^{3+}O_4$. *J. Phys. Chem. Solids* **1971**, *32*, 717–729. [CrossRef]
10. Levinstein, H.J.; Robbins, M.; Capio, C. A Crystallographic Study of the System $FeCr_2O_4$ Fe_3O_4 ($Fe^{2+}Fe^{3+}{}_xCr_{2-x}O_4$). *Mater. Res. Bull.* **1972**, *7*, 27–34. [CrossRef]
11. Ma, J.; Garlea, V.O.; Rondinone, A.; Aczel, A.A.; Calder, S.; dela Cruz, C.; Sinclair, R.; Tian, W.; Chi, S.; Kiswandhi, A.; et al. Magnetic and Structural Phase Transitions in the Spinel Compound $Fe_{1+x}Cr_{2-x}O_4$. *Phys. Rev. B* **2014**, *89*, 134106. [CrossRef]
12. Kose, K.; Iida, S. Interacting Phase Transitions in $Fe_{1+x}Cr_{2-x}O_4$ ($0 \leq x \leq 0.4$). *J. Appl. Phys.* **1984**, *55*, 2321–2323. [CrossRef]
13. Brown, R.A.; Bevan, S.C. The Thermal Decomposition of Ferrous Oxalate Dihydrate. *J. Inorg. Nucl. Chem.* **1966**, *28*, 387–391. [CrossRef]
14. Mohamed, M.A.; Galwey, A.K. A Kinetic and Mechanistic Study of the Isothermal Decomposition of Ferrous Oxalate Dihydrate. *Thermochim. Acta* **1993**, *213*, 269–278. [CrossRef]
15. Hermanek, M.; Zboril, R.; Mashlan, M.; Machala, L.; Schneeweiss, O. Thermal Behaviour of Iron(II) Oxalate Dihydrate in the Atmosphere of Its Conversion Gases. *J. Mater. Chem.* **2006**, *16*, 1273. [CrossRef]
16. Matsnev, M.E.; Rusakov, V.S. SpectrRelax: An Application for Mössbauer Spectra Modeling and Fitting. *AIP Conf. Proc.* **2012**, *1489*, 178–185. [CrossRef]
17. Rodríguez-Carvajal, J. Recent Advances in Magnetic Structure Determination by Neutron Powder Diffraction. *Phys. B Condens. Matter* **1993**, *192*, 55–69. [CrossRef]
18. Lacroix, C.; Mendels, P.; Mila, F. (Eds.) *Introduction to Frustrated Magnetism*; Springer: Berlin/Heidelberg, Germany, 2011. [CrossRef]
19. Joy, P.A.; Date, S.K. Comparison of the Zero-Field-Cooled Magnetization Behavior of Some Ferromagnetic and Ferrimagnetic Systems. *J. Magn. Magn. Mater.* **2000**, *218*, 229–237. [CrossRef]
20. Lotgering, F.K. On the ferrimagnetism of some sulphides and oxides. *Philips Res. Rep.* **1956**, *11*, 190–249.
21. Jacobs, I.S. High Field Magnetization Study of Ferrimagnetic Arrangements in Chromite Spinels. *J. Phys. Chem. Solids* **1960**, *15*, 54–65. [CrossRef]
22. Goldanskii, V.I.; Herber, R.H. *Chemical Applications of Mossbauer Spectroscopy*; Academic Press: San Diego, CA, USA, 1968.
23. Chen, Y.-L.; Yang, D.-P. *Mössbauer Effect in Lattice Dynamics*; Wiley-VCH: Weinheim, Germany, 2007.
24. Kaul, S.N. Static Critical Phenomena in Ferromagnets with Quenched Disorder. *J. Magn. Magn. Mater.* **1985**, *53*, 5–53. [CrossRef]
25. Hartmann-Boutron, F.; Imbert, P. Mössbauer Study of the Electronic and Magnetic Properties of Fe^{2+} Ions in Some Spinel-Type Compounds. *J. Appl. Phys.* **1968**, *39*, 775–785. [CrossRef]
26. Reimers, J.N.; Greedan, J.E.; Björgvinsson, M. Critical Properties of Highly Frustrated Pyrochlore Antiferromagnets. *Phys. Rev. B* **1992**, *45*, 7295–7306. [CrossRef] [PubMed]